The Analysis of Microwave Weather Project Data

M. S. Reid
Communications Elements Research Section

The Microwave Weather Project forms part of an overall Radio Systems Development Project which seeks to optimize the spacecraft-to-ground communications link. Statistical correlations of weather and communications capability at X- and K-bands are needed to provide practical statistical prediction of the performance of the Deep Space Network at X-band and, in the future, at K-band. A previous article discussed the general approach of the project, the measurements, calibrations, equipment, and methods. This article summarizes the results of the Weather Project for 1971 through 1974. Computed results of increases in system temperature due to atmospheric effects are plotted as functions of time, frequency, elevation angle, etc. Comparisons are made with theoretical predictions derived from a contractor report submitted to JPL, which calculated signal attenuation due to cloud cover from meteorological measurements.

I. Introduction

The Microwave Weather Project forms part of an overall Radio Systems Development Project which seeks to optimize the spacecraft-to-ground communications link. Statistical correlations of weather and communications capability at X- and K-bands are needed to provide practical statistical prediction of the performance of the DSN at X-band and, in the future, at K-band. A previous article (Ref. 1) discussed the general approach of the project, the measurements, calibrations, equipment, and methods. Problems encountered were also discussed as well as their possible solutions. This article summarizes the results of the Weather Project for calender years (CY) 1971 through 1974. Comparisons are made with theoretical predictions derived from a contractor report submitted to JPL, which calculated signal attenuation due to cloud cover from meteorological measurements (Ref. 2).

II. Equipment, Measurements, and Methods

A previous article (Ref. 1) discussed the equipment, the calibrations, the measurements, and the methods. For most of the recording period, CY 1971–1974, the

equipment used was the X- and K-band total power radiometers in the Multiple-Frequency X- and K-Band (MXK) feed cone and the S-band total power radiometers in the S-Band Megawatt Transmit (SMT) or Polarization Diversity S-Band (PDS) feed cones. These radiometers were operated for the Microwave Weather Project on a continuous basis, except for periods when it was not possible to operate and record data.

Time, antenna elevation angle, and system operating noise temperature were recorded once per minute for each frequency. The analysis of the data consisted of sorting the recorded information into elevation angle ranges (6–15, 25–45, and 45–90 deg) and into time periods (years, quarter years (seasons), and months), and computing percent of time that the system operating noise temperature was above a baseline for each frequency and for each time period and elevation angle range. The baseline noise temperature for each frequency is defined as that system operating noise temperature expected in clear, dry weather at any given antenna elevation angle. The baseline is thus the lowest system temperature that can be measured with a given instrumentation in a given configuration as a function of elevation angle.

All recorded data were carefully quality controlled. Data suspected of contamination with interference or with errors due to equipment or recording problems were excluded from the data set. Thus, as far as it was possible to ensure, all computed excess system temperatures (defined as recorded system temperature minus the baseline system temperature for the given elevation angle) were due to weather effects only. Certain contaminating effects, such as some station maintenance procedures on the antenna, minor detuning of receivers, etc., were difficult to distinguish from atmospheric effects, and therefore perfect data quality control cannot be guaranteed. However, as far as was possible to determine, no real weather effects were excluded and no extraneous effects were included.

III. Results

Figure 1 is a summary of the entire data set for S-, X- and K-bands for the calender year period 1971 through 1974. This is a probability distribution of the relative increase in system temperature and is averaged over all antenna elevation angles. The relative increase in system temperature (excess system temperature) is plotted in kelvins against percent of time. The reference system temperature against which the excess was measured was the baseline profile for each frequency, as discussed above.

The baseline was an average profile for each frequency, measured and computed over the several possible antenna and other equipment configurations. This has been discussed in detail elsewhere (Ref. 1). Different system configurations yielded different baselines, and as it was not possible to record all equipment interchanges and configuration changes, an average baseline over the time period was computed and used in the data analysis. The effect of using an average baseline rather than a measured baseline for each configuration was to reduce the resolution on excess system temperature measurement. The figure shows that the best resolution was 10 K at any elevation angle. The zenith values for the baseline were 25 K at S-band, 27.5 K at X-band, and 36 K at K-band.

Figures 2 through 5 show the same data separated by calender years. These four figures show the variable nature of atmospheric effects. Goldstone had a particularly bad year in 1971 with an unusually heavy and protracted snowstorm, while 1972 was a mild year from the point of view of atmospheric degradation.

Other effects must be taken into account when examining the results. Not only were different amounts of data recorded at the different frequencies but different amounts of data were recorded in different calender years as well. Furthermore, data at the different frequencies were not necessarily recorded at the same time. On the average, S-band and K-band data were simultaneously recorded with X-band data between 30 percent and 40 percent of the time.

Figures 6 through 8 present the same data separated by frequency and calender year.

In order to separate the different magnitudes of atmospheric noise temperature degradation by season, the data were plotted by frequency and quarter. Figure 9 shows the probability distribution of relative increase in system temperature for S-Band, averaged over all elevation angles and averaged over calender years 1971 through 1974, but separated into quarters. Figures 10 and 11 are similar plots for X-band and K-band, respectively.

Figure 12 shows a comparison between theoretical and measured X-band system temperature degradations as a function of elevation angle for one percent probability conditions. The dashed curves have been taken from the theoretical study of cloud effects referred to above (Ref. 2). The solid curves are taken from measured zenith elevation angle X-band data for Goldstone, averaged over calender years 1971 through 1974. These zenith, X-band data for one percent probability conditions were plotted

as a function of elevation angle by the cosecant law. (The theoretical curves were also plotted by the cosecant law.) It may be seen from the figure that the spread of the measured data is greater than the spread of the theoretical data. It must be noted, however, that the theoretical data are for clouds only, whereas the measured data were taken in all possible weather conditions.

The average number of events per year is plotted in Fig. 13 for the S-, X-, and K-bands. An event is a degradation in system operating noise temperature due to atmospheric effects. A system temperature degradation of 3 dB, for example, indicates that the system temperature doubled. The degradation of system temperature in kelvins is therefore a function of elevation angle. The curves in Fig. 13 are averaged over all elevation angles and over calender years 1971 through 1974. They show, for example, that a 3 dB degradation in system temperature, at any elevation angle, occurs an average 3 times per year at S-band, 6.7 times per year at X-band, and 52 times per year at K-band.

Figure 14 shows the average time duration in minutes of system temperature degradation events. The data in Fig. 14 are averaged for 1971 through 1974 and averaged over all elevation angles.

The same cautions should be observed with Figs. 13 and 14 as were noted with all the previous figures.

Figures 15 and 16 show the probability distributions of relative increase in system temperature as a function of antenna elevation angle at S- and X-bands, respectively. These curves are averaged over 1971 through 1974 and show the differences in degradation effects at different elevation angle ranges.

IV. Conclusions

The results show that higher resolution is a desirable goal. The lack of resolution is due to the averaging of the baselines. An average baseline was mandatory because of a lack of recording capability on configuration changes. These configuration changes included subreflector position, diplexed or low noise operation, reflex or retracted microwave optics, receiver bandwidth changes and operating frequency changes. Most, but not all, X-band data were taken at 7840, 8415, or 8448 MHz. Most, but not all, K-band data were taken at 14.5, 14.7, or 15.3 GHz. Other effects, which led to reduced resolution due to the introduction of contaminated data, were fourth harmonic interference at X-band by the S-band transmitter breakthrough, receiver tests injecting a continuous-wave (CW) signal level in the intermediate frequency (IF) pass-band, maser gain drifts, etc.

In order to acquire high resolution data, a noise-adding radiometer system at X-band has been built and installed at the Goldstone Venus Station (DSS 13) for the recording of weather data. This is a gain-stabilized system with careful temperature control on all sensitive components and which operates continuously supplying data to an automatic data acquisition system (Ref. 3). This X-band radiometer system has been described in detail elsewhere (Ref. 4) and will be supplemented by a K-band (15 GHz) system in the near future.

References

1. Reid, M. S., "A Description of the Weather Project," in *The Deep Space Network Progress Report*, Technical Report 32-1526, Vol. X, pp. 116–122, Jet Propulsion Laboratory, Pasadena, Calif., Aug. 15, 1972.
2. Smith, T. B., and Chien, C. W., *Cloud Cover Effects on Signal Attenuation at DSN Sites*, Subcontract No. 952757, Meteorology Research Inc., Altadena, Calif., Apr. 1970.
3. Reid, M. S., and Gardner, R. A., "A Versatile Data Acquisition System for Goldstone," in *The Deep Space Network Progress Report 42-30*, pp. 132–143, Jet Propulsion Laboratory, Pasadena, Calif., Dec. 15, 1975.
4. Reid, M. S., Parham, O. B., and Gardner, R. A., "An X-Band Radiometer for the Microwave Weather Project" in *The Deep Space Network Progress Report 42-29*, pp. 54–59, Jet Propulsion Laboratory, Pasadena, Calif., Oct. 15, 1975.

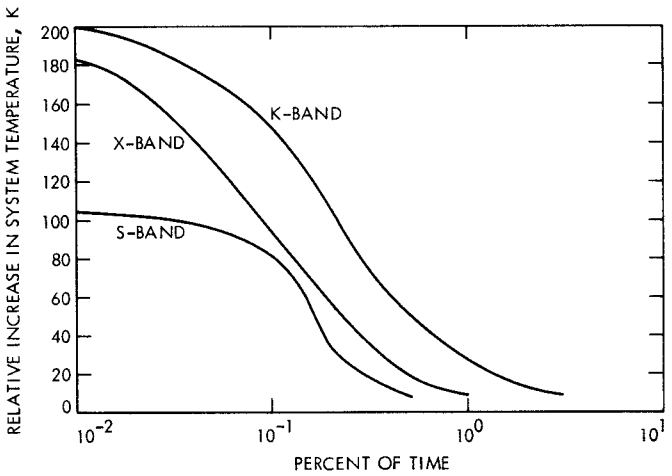

Fig. 1. Probability distribution of relative increase in system temperature: 1971 through 1974 averages for S-, X-, and K-bands

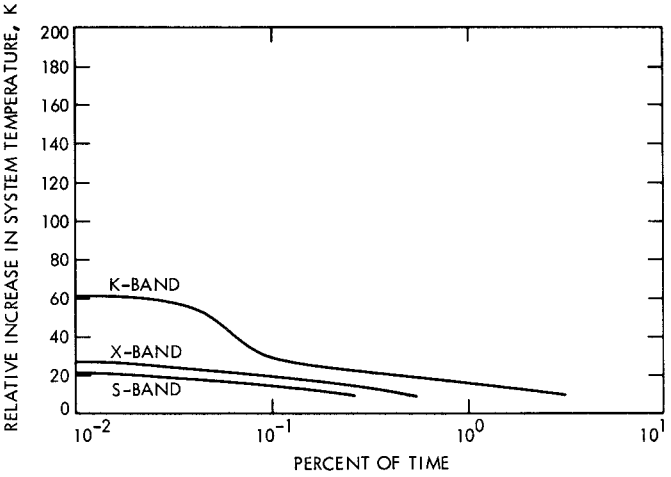

Fig. 3. Probability distribution of relative increase in system temperature for calendar year 1972

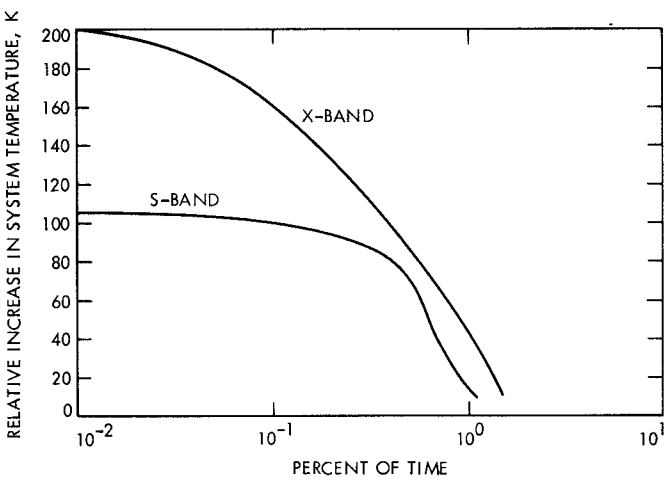

Fig. 2. Probability distribution of relative increase in system temperature for calendar year 1971

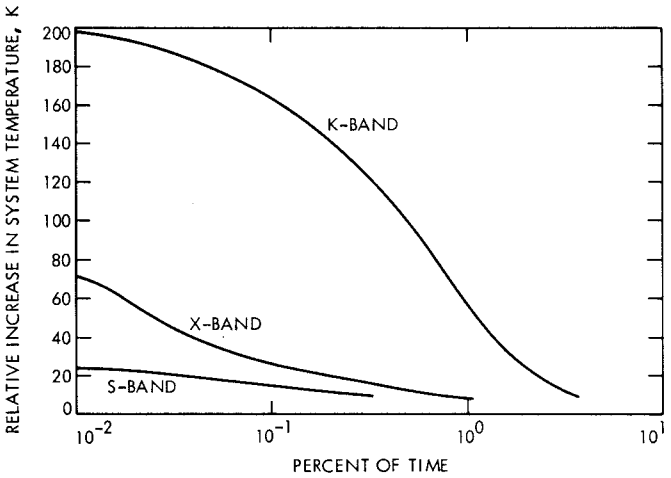

Fig. 4. Probability distribution of relative increase in system temperature for calendar year 1973

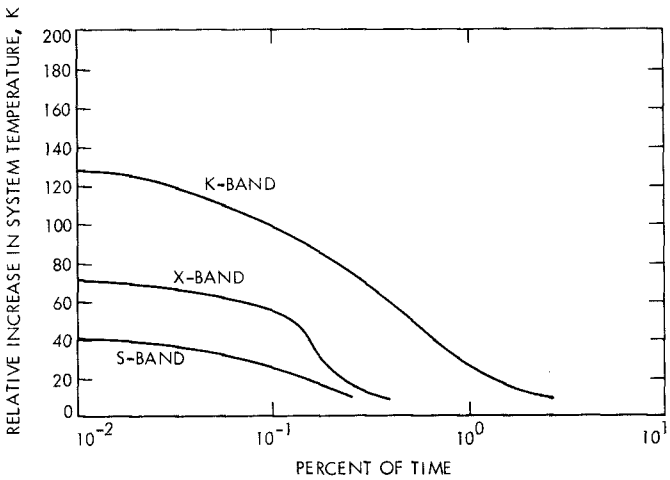

Fig. 5. Probability distribution of relative increase in system temperature for calendar year 1974

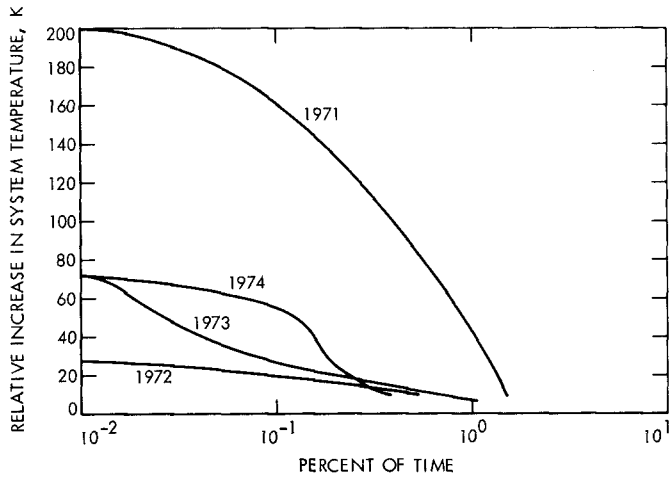

Fig. 7. Probability distribution of relative increase in system temperature for X-band for calendar years 1971 through 1974

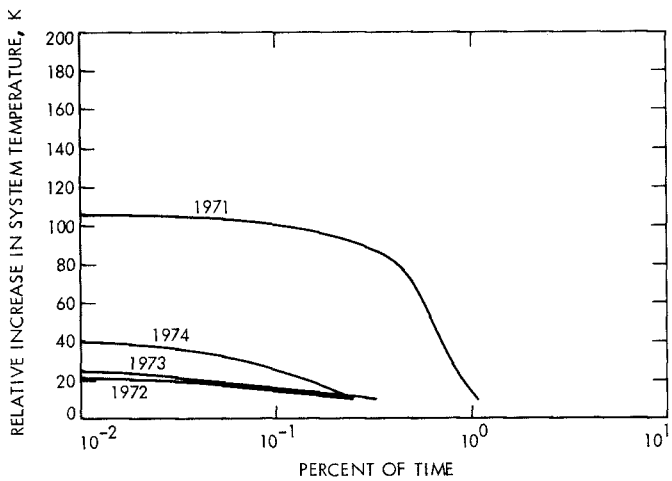

Fig. 6. Probability distribution of relative increase in system temperature for S-band for calendar years 1971 through 1974

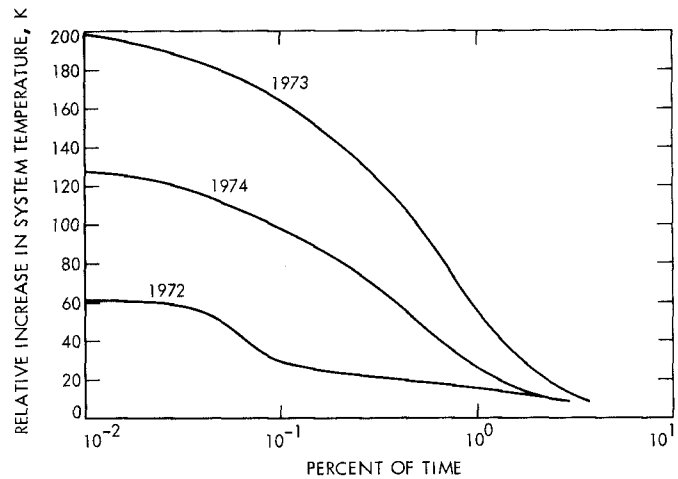

Fig. 8. Probability distribution of relative increase in system temperature for K-band for calendar years 1972 through 1974

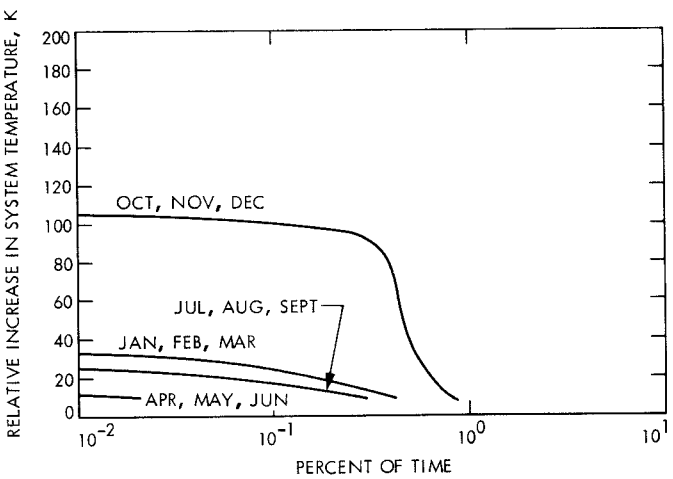

Fig. 9. Probability distribution of relative increase in system temperature for S-band by season

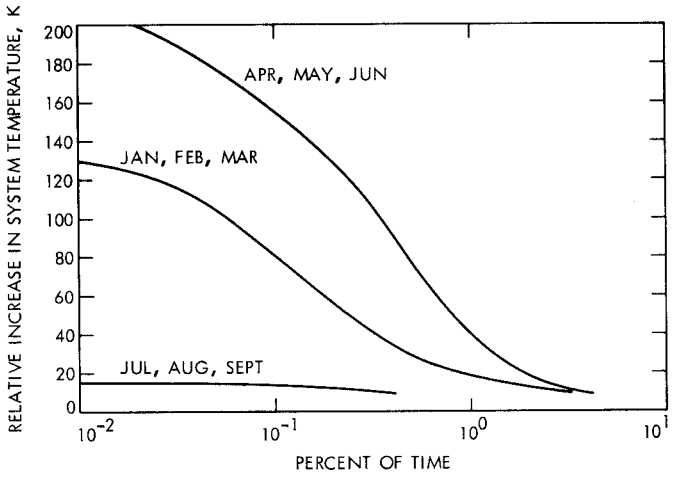

Fig. 11. Probability distribution of relative increase in system temperature for K-band by season

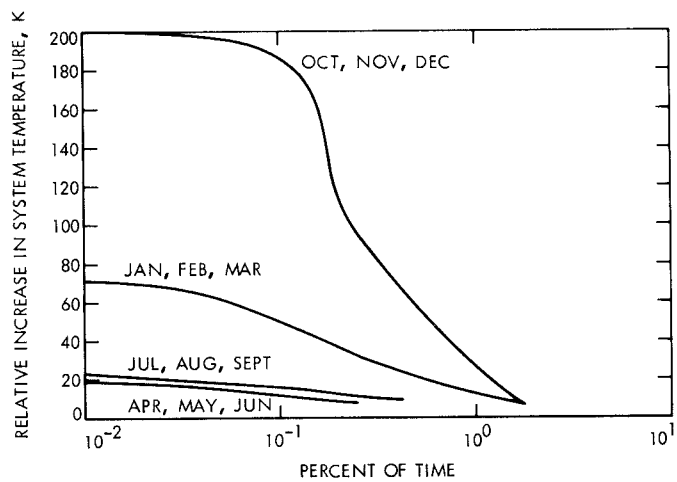

Fig. 10. Probability distribution of relative increase in system temperature for X-band by season

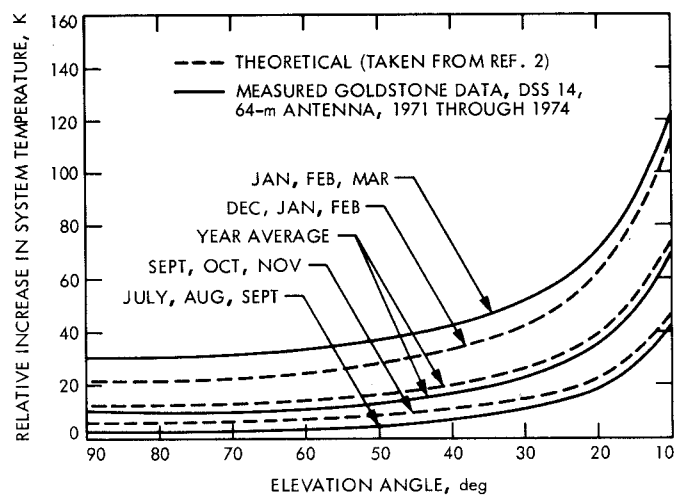

Fig. 12. Theoretical and measured relative increase in system temperature at X-band due to the atmosphere at Goldstone for one percent probability conditions

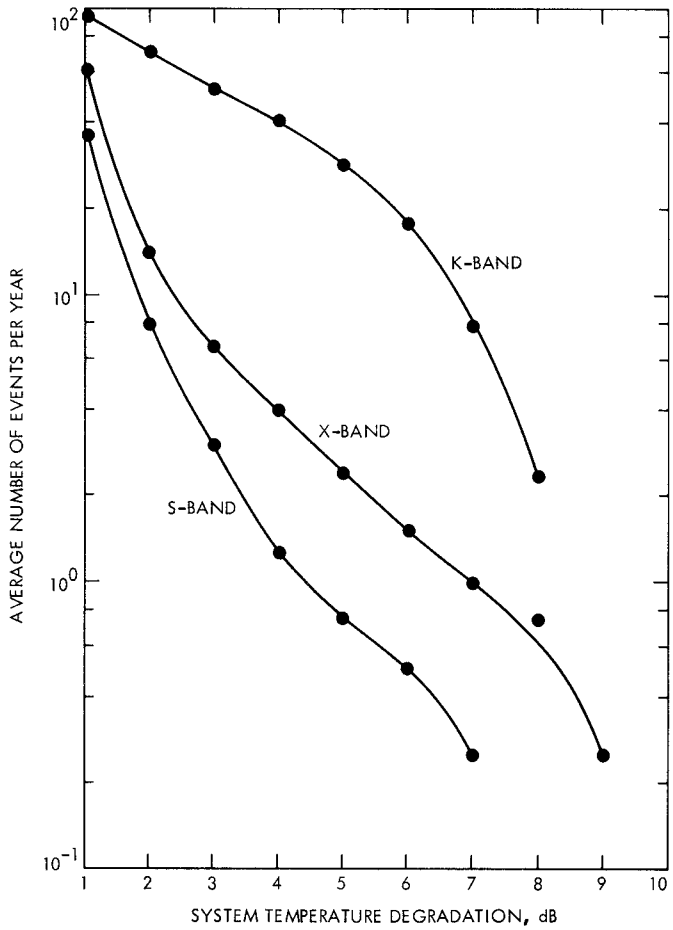

Fig. 13. Average number of system temperature degradation events per year for S-, X-, and K-bands

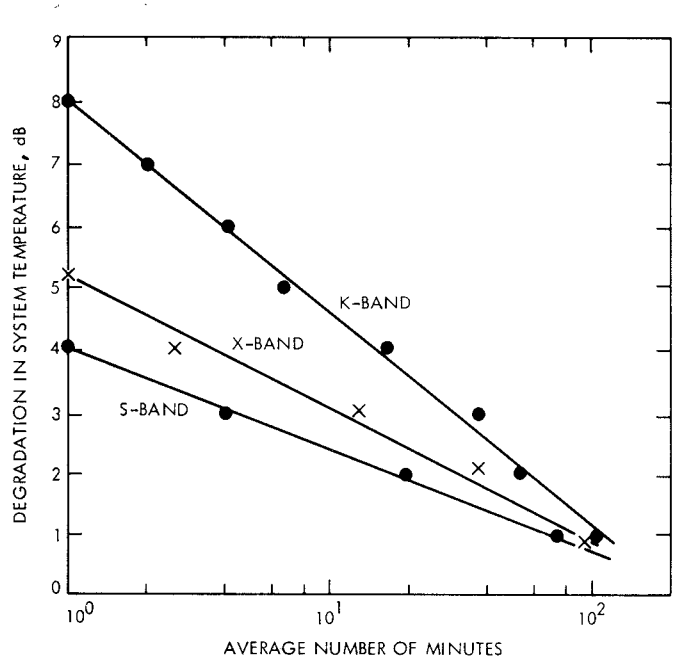

Fig. 14. Average time duration of system temperature degradation events for S-, X-, and K-band

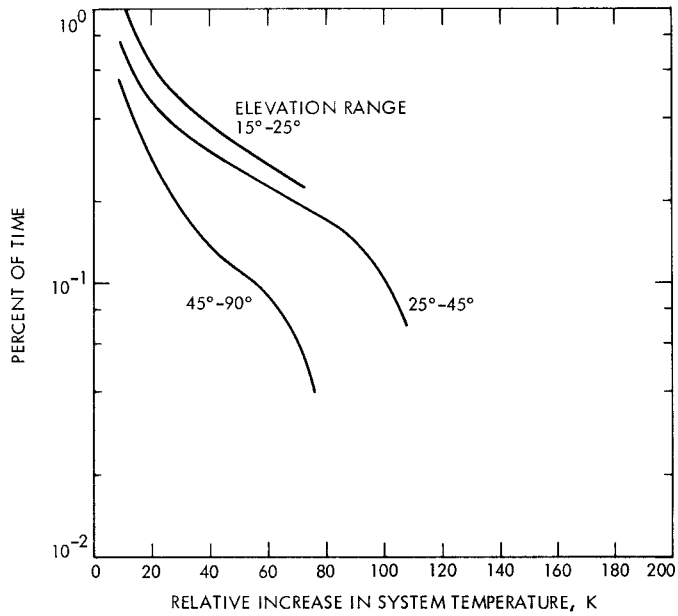

Fig. 15. Probability distribution of relative increase in system temperature for S-band as a function of elevation angle

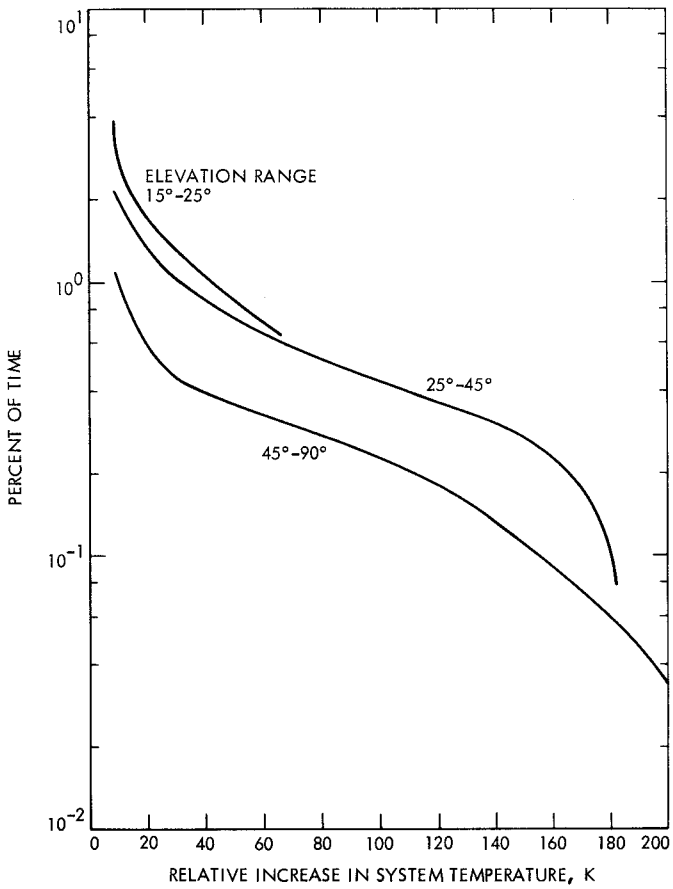

Fig. 16. Probability distribution of relative increase in system temperature for X-band as a function of elevation angle